

Camera array based light field microscopy

Xing Lin,^{1,2} Jiamin Wu,^{1,2} Guoan Zheng,³ and Qionghai Dai^{1,2,*}

¹Department of Automation, Tsinghua University, Beijing, 100084, China

²Beijing Key Laboratory of Multi-dimension & Multi-scale Computational Photography (MMCP), Tsinghua University, Beijing, 100084, China

³Biomedical Engineering & Electrical Engineering, University of Connecticut, Storrs, Connecticut, 06269, USA

[*qionghaidai@mail.tsinghua.edu.cn](mailto:qionghaidai@mail.tsinghua.edu.cn)

Abstract: This paper proposes a novel approach for high-resolution light field microscopy imaging by using a camera array. In this approach, we apply a two-stage relay system for expanding the aperture plane of the microscope into the size of an imaging lens array, and utilize a sensor array for acquiring different sub-apertures images formed by corresponding imaging lenses. By combining the rectified and synchronized images from 5 × 5 viewpoints with our prototype system, we successfully recovered color light field videos for various fast-moving microscopic specimens with a spatial resolution of 0.79 megapixels at 30 frames per second, corresponding to an unprecedented data throughput of 562.5 MB/s for light field microscopy. We also demonstrated the use of the reported platform for different applications, including post-capture refocusing, phase reconstruction, 3D imaging, and optical metrology.

© 2015 Optical Society of America

OCIS codes: (180.6900) Three-dimensional microscopy; (110.1758) Computational imaging; (170.0110) Imaging systems; (100.3010) Image reconstruction techniques.

References and links

- M. Levoy, R. Ng, A. Adams, M. Footer, and M. Horowitz, "Light field microscopy," *ACM Trans. Graph.* **25**(3), 924–934 (2006).
- R. Prevedel, Y. Yoon, M. Hoffmann, N. Pak, G. Wetzstein, S. Kato, T. Schrödel, R. Raskar, M. Zimmer, E. S. Boyden, and A. Vaziri, "Simultaneous whole-animal 3D imaging of neuronal activity using light-field microscopy," *Nat. Methods* **11**(7), 727–730 (2014).
- G. Lippmann, "La Photographie Intégrale," *Academie des Sciences* **146**, 446–451 (1908).
- M. Levoy, Z. Zhang, and I. McDowell, "Recording and controlling the 4D light field in a microscope using microlens arrays," *J. Microsc.* **235**(2), 144–162 (2009).
- M. Broxton, L. Grosenick, S. Yang, N. Cohen, A. Andelman, K. Deisseroth, and M. Levoy, "Wave optics theory and 3-D deconvolution for the light field microscope," *Opt. Express* **21**(21), 25418–25439 (2013).
- N. Cohen, S. Yang, A. Andelman, M. Broxton, L. Grosenick, K. Deisseroth, M. Horowitz, and M. Levoy, "Enhancing the performance of the light field microscope using wavefront coding," *Opt. Express* **22**(20), 24817–24839 (2014).
- S. Dong, R. Horstmeyer, R. Shiradkar, K. Guo, X. Ou, Z. Bian, H. Xin, and G. Zheng, "Aperture-scanning Fourier ptychography for 3D refocusing and super-resolution macroscopic imaging," *Opt. Express* **22**(11), 13586–13599 (2014).
- L. Tian, J. Wang, and L. Waller, "3D differential phase-contrast microscopy with computational illumination using an LED array," *Opt. Lett.* **39**(5), 1326–1329 (2014).
- G. Zheng, R. Horstmeyer, and C. Yang, "Wide-field, high-resolution Fourier ptychographic microscopy," *Nat. Photonics* **7**(9), 739–745 (2013).
- A. Orth, and K. B. Crozier, "Light field moment imaging," *Opt. Lett.* **38**(15), 2666–2668 (2014).

11. A. Levin, W. T. Freeman, and F. Durand, "Understanding Camera Trade-Offs through a Bayesian Analysis of Light Field Projections," in *Proceedings of the ECCV* (Springer, 2008) pp. 88-101.
 12. T. E. Bishop, and P. Favaro, "The light field camera: Extended depth of field, aliasing and superresolution," *IEEE Trans. Pattern Anal. Mach. Intell.* **34**(5), 972–986 (2012).
 13. A. Lumsdaine, and T. Georgiev, "The focused plenoptic camera," in *Proceedings of the ICCP* (IEEE, 2009), pp. 1–8.
 14. C. Lu, S. Muenzel, and J. Fleischer, "High-resolution light-field microscopy," in *Computational Optical Sensing and Imaging, Microscopy and Tomography I* (2013), CTh3B.
 15. K. Marwah, G. Wetzstein, Y. Bando, and R. Raskar, "Compressive light field photography using overcomplete dictionaries and optimized projections," *ACM Trans. Graph.* **32**(4), 1–11 (2013).
 16. I. Tosic, S. A. Shroff, and K. Berkner, "Dictionary learning for incoherent sampling with application to plenoptic imaging," in *Proceedings of the ICASSP* (IEEE, 2013), pp. 1821–1825.
 17. A. W. Lohmann, R. G. Dorsch, D. Mendlovic, Z. Zalevsky, and C. Ferreira, "Space-bandwidth product of optical signals and systems," *J. Opt. Soc. Am. A* **13**(3), 470–473 (1996).
 18. D. J. Brady, M. E. Gehm, R. A. Stack, D. L. Marks, D. S. Kittle, D. R. Golish, E. M. Vera, and S. D. Feller, "Multiscale gigapixel photography," *Nat.* **486**(7403), 386–389 (2012).
 19. V. Vaish, B. Wilburn, N. Joshi and M. Levoy, "Using plane + parallax for calibrating dense camera arrays," in *Proceedings of the CVPR* (IEEE, 2004), pp. 2–9.
 20. X. Lin, J. Suo, G. Wetzstein, Q. Dai and R. Raskar, "Coded focal stack photography," in *Proceedings of the ICCP* (IEEE, 2013), pp. 1–9.
 21. J. Wu, X. Lin, Y. Liu, J. Suo, and Q. Dai, "Coded aperture pair for quantitative phase imaging," *Opt. Lett.* **39**(19), 5776–5779 (2014).
-

1. Introduction

Light field microscopy (LFM) [1] is a scanless 3D computational imaging approach that records both 2D spatial and 2D angular distribution of light passing through a specimen. This kind of spatio-angular data allows for computationally synthesizing focal stacks, flexibly controlling depth of field and achieving full volumetric reconstruction, and hence has important applications in optical bioimaging [2]. The current optical schematic of LFM, which can be dated back to 1908 by Lippmann [3], is implemented by inserting a microlens array at the intermediate image plane of an optical microscope so that sensor pixels capture the rays of 4D light field during a single exposure. However, microlens array based light field microscopy (MALM) suffers from inherent trade-offs between sensor spatial resolution and angular resolution measurement [4], which degrades the final achievable image resolution by orders of magnitude compared with the raw sensor resolution.

To address the drawback of the decreased spatial resolution of LFM, 3D deconvolution [5] has been proposed to reconstruct volumetric data with improved spatial resolution, which requires a computationally intensive process and results in non-uniform lateral resolution across the depth of field. The resulting non-uniform lateral resolution across the depth of field can be mitigated with additional phase masks for wavefront coding [6]. Accounting for the application of high-resolution post-capture refocusing, aperture scanning [7] or LED scanning methods [8, 9] can be employed alternatively to achieve full sensor resolution digital refocusing at the sacrifice of temporal resolution. By incorporating prior knowledge about the object, for example, Gaussian angular distribution assumption for light field moment imaging [10, 11], Lambertian reflectance priors with super-resolution [12–14] or learning an over-complete dictionary to exploit its intrinsic redundancy [15, 16], high-resolution light fields can be computationally reconstructed. Unfortunately, these empirical assumptions do not always hold for microscopic samples.

In this paper, we report a new LFM configuration for addressing the intrinsic resolution trade-offs of the conventional LFM. The reported approach, termed *camera array based light field microscopy (CALM)*, utilizes a 5×5 camera array to simultaneously capture different perspective images of the sample, corresponding to different sub-apertures of the two-stage relay system. We show that high-resolution light fields can be obtained by simply rectifying the

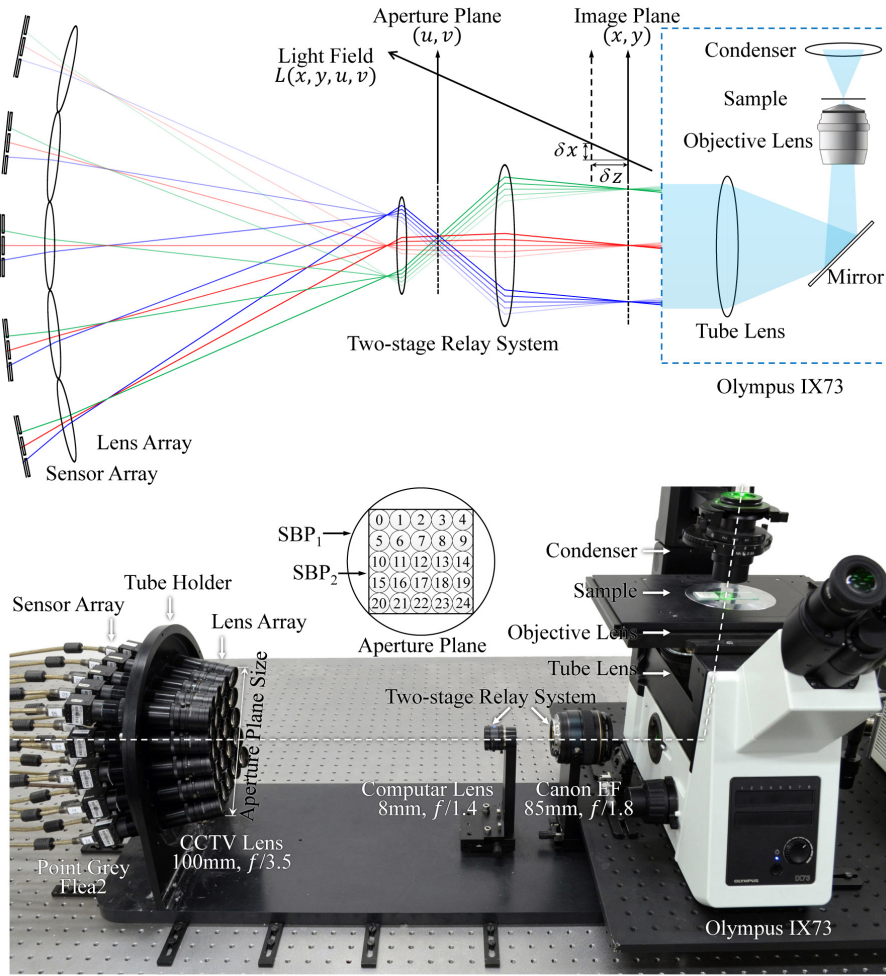


Fig. 1. Schematic of the proposed CALM system (top) and a photograph showing the prototype system (bottom) ([Visualization 1](#)). We employed 25 cameras to capture the color light field videos of the microscopic specimens with a spatial resolution of 0.79 megapixels at 30 frames per second. The light microscope (Olympus IX73) is configured with a objective lens with 10 \times magnification, 0.4 numerical aperture and 2.65mm field-of-view.

captured sub-aperture images without further processing or enforcing any prior assumptions on the microscopic specimens.

We provide three key insights on the optical system comparison between our approach and the MALM as follows:

First, our approach can achieve much higher data transmission capability by using a parallel data acquisition and storage scheme. The space-bandwidth product (SBP) [17] of an optical system places an upper bound on the product of spatial and angular resolution in light fields (i.e. the total pixel count of employed sensors). Conventional microscope objective has a SBP of tens of mega-pixels, on the same order of pixel number of conventional image sensor. However, higher SBP lens system exists [18], for example, the SBP of Olympus MVX10 stereoscopic objective lens (MVPLAPO2XC) is approximate 0.7 billion; and a simple closed-circuit television (CCTV) lens reported in [7] has a SBP of 0.5 billion which is orders of magnitude higher than

existing sensor resolution. In this regard, CALM can achieve higher resolution and higher SBP by using a camera sensor array at detection path. In contrast, MALM utilizes a single sensor and the final achievable SBP is determined by the sensor, not the employed optics.

Second, our approach provides more flexible optical configurations. Perspective images are highly redundant and humans are more tolerant of low angular resolution than low spatial resolution [1]. Under a SBP-limited objective lens, CALM can be easily configured to capture low angular but high spatial resolution light fields, while it is challenging for MALM to manufacture the microlens array with small pitch and suitable focal length for the same goal. On the other hand, under a high SBP objective lens, utilizing a microlens array with large pitch to increase the angular resolution will reduce the final spatial resolution of light field; however, capturing more angular resolutions can be simply implemented by adding more cameras in our approach without sacrificing the spatial resolution.

Third, compared with MALM that employs a single camera, the parameters of each camera in CALM can be set independently for different applications, such as compensating the angularly non-uniform illumination or inconsistent focal positions. Marginal views usually have lower light intensity compared with center views, especially when the numerical aperture of the illumination is smaller than that of the employed objective lens. In our approach, the uniform illuminated light field images can be obtained by setting different exposure time for different perspective views. By setting different focal positions for different cameras and placing them at a curved surface, we can correct for the non planar focal aberration of the objective lens.

2. Light field imaging using a camera array

In this section, we will first demonstrate the optical schematic of the our CALM prototype in Section 2.1. We will then evaluate the imaging performance using a USAF resolution target in Section 2.2

2.1. System design of the CALM

Figure 1 shows a schematic of the proposed optical system and a photograph of the prototype system. To facilitate the prototype system building, we adopted a commercially available inverted microscope (Olympus IX73) for producing a magnified image of the specimen at the image plane. A partially coherent white LED light source with a green interference filter (central wavelength $\lambda = 550 \text{ nm}$) is used to provide illumination for the system, and the numerical aperture of the condenser lens is 0.55. We used a $10\times$ air objective lens (Olympus, UPLSAPO10X2, $N.A. = 0.4$, $F.N. = 26.5$) for all experiments in this paper. The image plane of microscope is relayed by a two-stage relay system to form the aperture plane whose diameter is equivalent to the diagonal line of the lens array, as shown in Fig. 1(bottom). The first-stage relay lens (Canon EF, 85 mm, $f/1.8$, USM) is used to generate the aperture plane and it is magnified by the second-stage relay lens (Computar M0814-MP2, 8 mm, $f/1.4$). The magnification factor is determined by the ratio of two focal lengths of the relay lens; and $N.A.$ is matched by keeping the $N.A.$ of the second-stage relay lens larger than the first-stage relay lens. Finally, we placed the imaging lens array (CCTV SV-10035V, 100 mm, $f/3.5$) at the aperture plane to obtain sub-aperture images that are recorded with the sensor array. The sensor is a PointGray Flea2-08S2C-C RGB color sensor with pixel pitch $4.65 \mu\text{m}$, operated at resolution 1024×768 pixels with frame rate 30 fps. Since the light propagation in our system is no longer under the paraxial approximation, we adopted the arc configuration of the sensor array in this implementation. The lens array and sensor array are placed on the spherical surface with its center at the second-stage relay lens. The radius of tube holder we used for fixing the camera array is 472mm in this design, which is determined with a single camera before the manufacture. Finally, we established the master-slave server architecture to synchronize between sensors, acquire large-capacity light

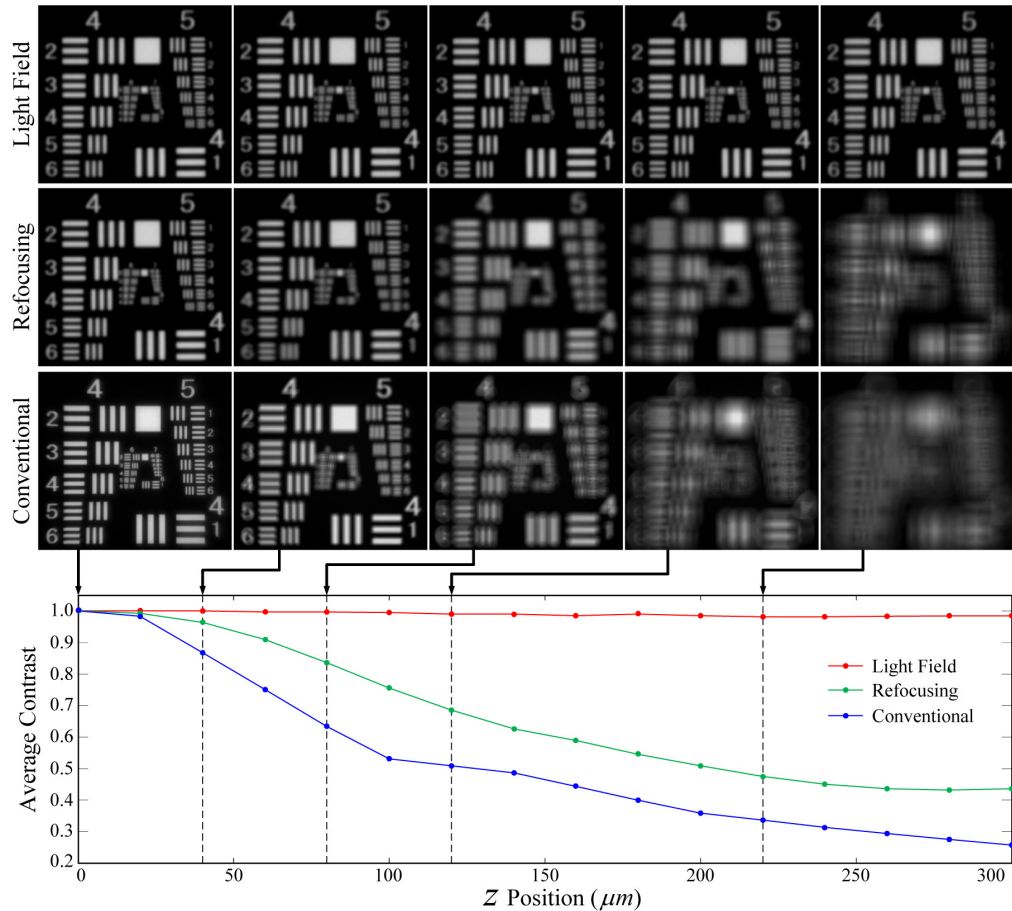


Fig. 2. Evaluating resolution and depth of field of the prototype system. The captured light fields have large depth of field (first row), and can achieve an optical sectioning comparable to conventional microscopy (third row) by combining 25 views for refocusing (second row). The axial resolution of our system is $8.8\mu m$ and the resolvable group of stripe for each view is 5.6 (line width $8.77\mu m$).

field videos and provide user interface ([Visualization 1](#)).

The SBP of a microscope objective can be given as

$$SBP = F.O.V / (0.5d)^2, \quad (1)$$

where $F.O.V = 0.25\pi(F.N./Magnification)^2$ is the field of view in the object plane; $d = 0.61\lambda/N.A.$ is the diffraction limit of resolution for the objective lens; and constant factor 0.5 comes from the Nyquist sampling theorem. As illustrated in Fig. 1(bottom), the SBP of the objective lens in our setup SBP_1 is about 31.3 mega-pixels and the SBP for camera array arranged as square in the center SBP_2 is about 19.9 mega-pixels. Therefore, we employed 25 sensors, which have the total number of 19.6 mega-pixels, to make full use of the information capacity of our optical system, resulting in 5×5 angular resolution in this implementation. And the $N.A.$ of imaging lenses are set to 1/7.0 (the effective $N.A.$, $f/\# = 7.0$) for $N.A.$ matching of the second-stage relay lens and reducing the ambient light. The system performs near the diffraction limit. Since the diffraction limit d of our objective lens is $0.84\mu m$, the lateral

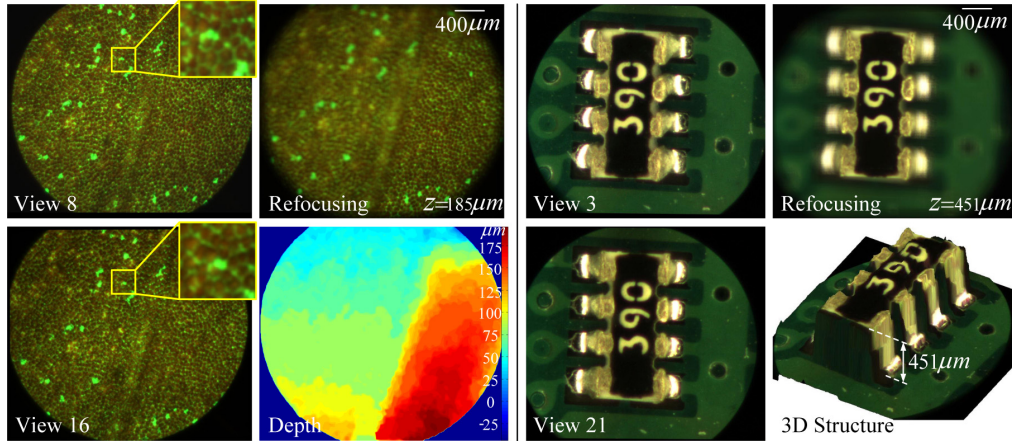


Fig. 3. Capturing the light field of rose petal (left, [Visualization 2](#)) and integrated circuit board (right, [Visualization 3](#)) for synthetic refocusing and recovering its 3D structure. The parallaxes of specimens for different views are successfully recorded (first and third column), which can be used for post-capture refocusing (second and fourth column, top) and 3D reconstruction (second and fourth column, bottom).

resolution imposed by diffraction limit is approximately $4.20\mu\text{m}$ for each view.

Since we used the same model sensors in our implementation, besides the focal position, we set other parameters (white balance, exposure time, gain, aperture size, etc) the same for all cameras to compensate for the difference. For geometric calibration, we first aligned the optical axis of the camera array, relay system and the camera port of microscope, and assembled the camera array by converging the optical axis of each camera to the center of the second-stage relay lens. During the assembly, we precisely adjusted the direction of each camera, glued its tube onto the tube holder and assembled cameras one by one. A checkerboard was mounted on the imaging plane during the calibration, and the captured perspective images were registered with the simple planar parallax procedure as described in [19] to obtain the rectified light field. Light field $L(x, y, u, v)$ describes a mapping from rays to radiance, as a function of position (x, y) and direction (u, v) in the free space (shown in Fig. 1(top)).

2.2. System characterization of the CALM

Synthetic refocusing is one of the most important applications of light field imaging, which can be implemented by shearing the 4D light field and projecting along its angular dimension [1]. The minimum refocusing step size along the axial dimension that determines the axial resolution of 3D reconstructions in this paper can be formulated as

$$\delta z = \delta x \cot(\arcsin(N.A.)) / M, \quad (2)$$

where δx represents the shearing of a single pixel size; $M = 1.21$ is the magnification of the optical system which is measured with the stage micrometer (OBM1/100, 1 mm/100 units). So $\delta z = 8.8\mu\text{m}$ and each pixel of the sensor corresponds to $3.84\mu\text{m}$ resolvable feature size in the object plane. The final lateral resolution for each view is $7.68\mu\text{m}$, which is determined by the sensor pixel size rather than the diffraction limit ($4.20\mu\text{m}$).

Figure 2 evaluates the resolution and depth of field of the prototype system by imaging a standard USAF 1951 resolution target and measuring the normalized average contrast from group 4.1 to group 5.6 of stripes [5]. We translated the focal plane above the native object plane

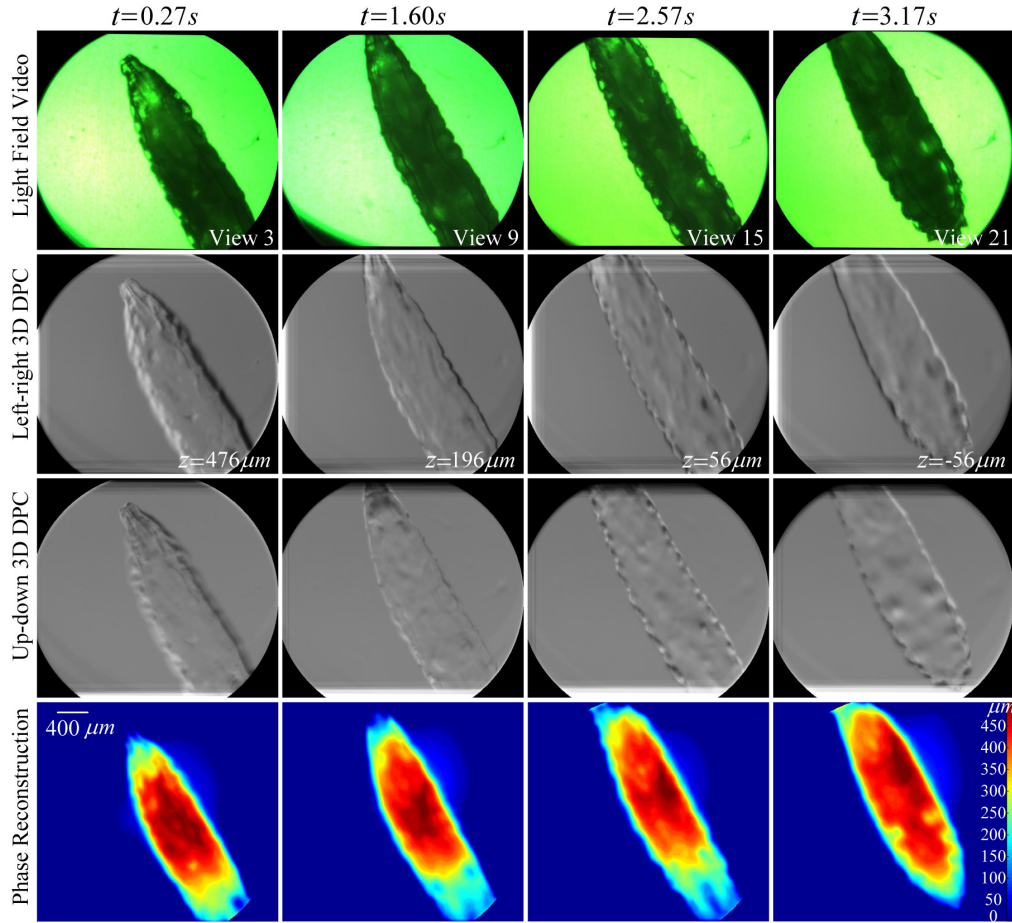


Fig. 4. The applications of light field video of drosophila larva to 3D DPC and phase reconstruction ([Visualization 4](#)). With the captured light field video of a living drosophila larva (first row), the 3D differential phase-contrast (DPC) video pair is computed (second and third rows) for recovering the phase video (forth row) which represents sample's optical path length (e.g. height).

($z = 0 \mu m$) in $20 \mu m$ increments, captured light fields at each increment and performed sample refocusing. Top row of Fig. 2 demonstrates the large focal range of our system. For the light field captured at $z = 0 \mu m$, we synthetically refocus it with $20 \mu m$ increment and compare it with the conventional microscopy in Fig. 2 (middle and bottom rows). Our synthetic refocusing images get out-of-focus quickly as expected, which is comparable to the conventional microscopy indicating the good optical sectioning of our system. Due to the optical aberration and sensor pixel size, the resolvable group of stripes for each view of our system and conventional microscopy are 5.6 (line width $8.77 \mu m$) and 6.6 (line width $4.38 \mu m$), respectively.

3. Experimental results

To demonstrate the imaging performance of the reported approach and its application to optical metrology, we capture the light field of a rose petal and an integrated circuit board as shown in Fig. 3. We used an epi-illumination configuration for capturing the integrated circuit board

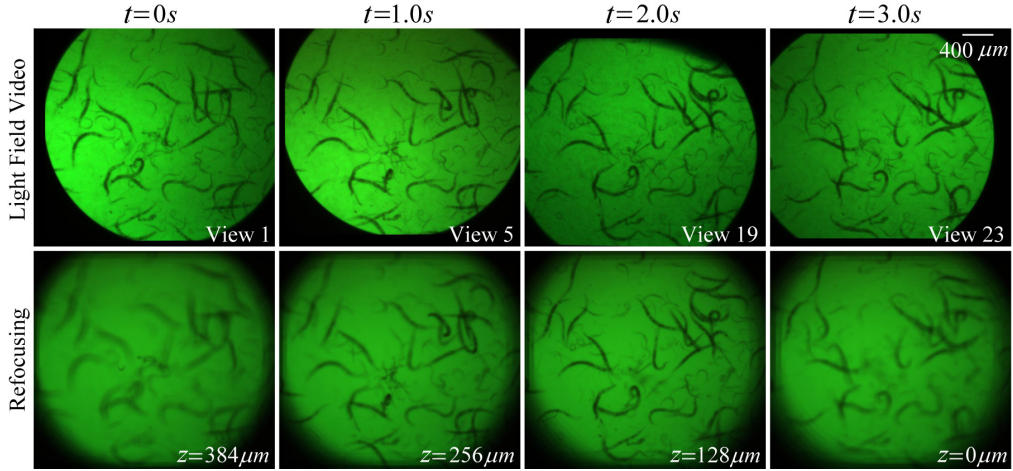


Fig. 5. The light field and synthetic refocusing videos of the *Caenorhabditis elegans* (*C. elegans*) in the water ([Visualization 5](#)). We captured the light field video of large scale *C. elegans* movement in the water (first row), and the synthetic refocusing video from it reveals the relative spatial locations of different *C. elegans* along the axial dimension (second row).

due to its opaque material property and applied a trans-illumination to other experiments in this paper. Since the diffuser used in the trans-illumination configuration hardly produces the isotropic illumination, the epi-illumination configuration achieves more uniform illumination for different views. The parallaxes for different views are successfully recorded (first and third column) and they allow for post-capture refocusing (second and fourth column, top). In order to facilitate the depth recovery without calibrating the intrinsic and extrinsic camera parameters, we applied the depth-from-defocus method [20] to estimating its depth and 3D structure from the synthesized defocused images (second and fourth column, bottom). The final spatial resolution of rose petal dataset is 880×768 . For the integrated circuit board dataset, the actual depth range measured by the vernier calipers is $459 \mu\text{m}$. It matches the depth range obtained by synthetic refocusing (front focus to rear focus) which is $451 \mu\text{m}$. The detailed 3D structures of the chromatic specimens are faithfully reconstructed ([Visualization 2](#) and [Visualization 3](#)).

Since the employed sensor has a frame rate of 30 fps, we conducted the light field video acquisition for various living specimens. Figure 4 demonstrates the light field video of a living drosophila larva ([Visualization 4](#)); and the movement of large numbers of *Caenorhabditis elegans* (*C. elegans*) in the water is shown in Fig. 5 ([Visualization 5](#)). The 3D differential phase-contrast (DPC) videos [8] of drosophila larva are computed as the normalized difference between opposite halves of the perspective images (Fig. 4(middle rows)), which indicates the two direction derivatives of the light field. It represents the object's phase gradient along the axis of asymmetry, so the phase can be quantitatively recovered from the gradient fields of DPC videos, with the result shown in Fig. 4(bottom row). Phase reconstruction results φ are displayed as the height h of the object in the axial dimension for better visualization, where $h = \varphi\lambda\Delta n/2\pi$ and Δn is the differential refractive index between the specimen and environment. Our quantitative phase retrieval video reveals the morphological changing of translucent drosophila larva body during its movement. The light field and synthetic refocusing videos of the *C. elegans* in Fig. 5 demonstrate the relative spatial locations of different *C. elegans* along the axial dimension.

We also quantitatively evaluate the accuracy of light fields captured by our approach in Fig. 6 ([Visualization 6](#)). We adopted a custom-made plano-convex microlens array, which is made of a plastic material (Cyclic Olefin Copolymer) with excellent optical properties, as the target

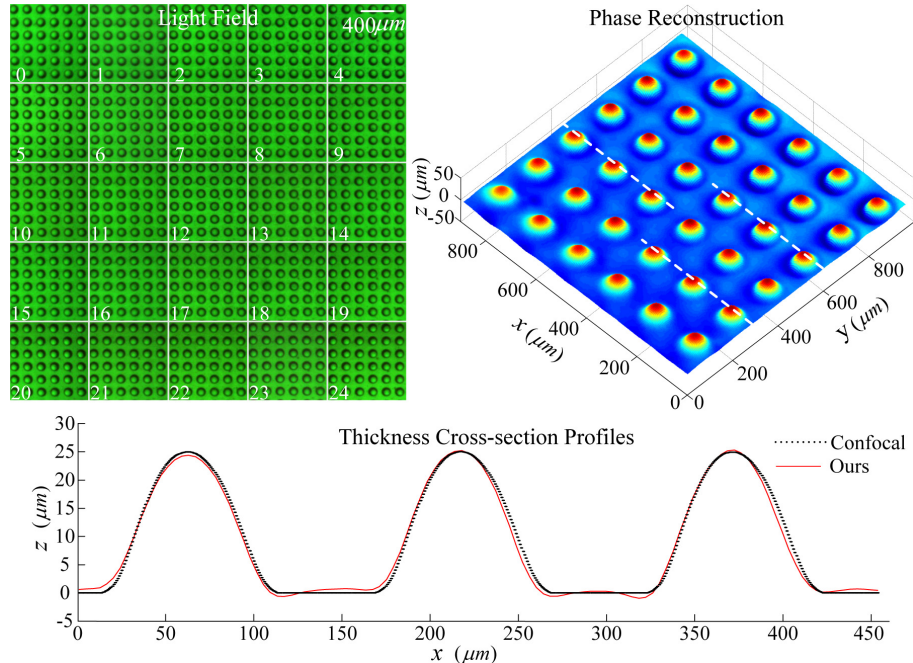


Fig. 6. Quantitative phase reconstruction for microlens array with the captured light field ([Visualization 6](#)). In order to quantitatively evaluate the accuracy of captured light fields by using our approach, we reconstructed the phase of a microlens array (top-right) with its snapshot light field (top-left) and compared the recovered shape with a scanning confocal light microscopy result (bottom).

sample ($100 \mu\text{m}$ pitch, refractive index $n = 1.53$). With the captured light field in Fig. 6(top-left), the phase of microlens array is quantitatively recovered as shown in Fig. 6(top-right) by using the method proposed in [21]. The normalized root-mean-square error (NRMSE) of the reconstructed shape with respect to the result measured by scanning confocal microscopy (Olympus FV1200) is 0.0851. In addition, the comparison of the microlens thickness cross-sections obtained by our approach (the average of three line profiles indicated in top-right) and confocal microscopy is shown in Fig. 6(bottom). The result indicates that our light field data can achieve high-accuracy phase reconstruction that has good agreement to the confocal microscopy.

4. Discussion

To the best of our knowledge, we are the first to apply a camera array for light field imaging in microscopy, which can achieve high-resolution and high frame rate light field videos acquisition with high accuracy. The optical schematics of camera array based light field imaging in macro-scenarios [19] and microscope are different. In microscopic imaging, we applies objective lens to magnify the specimen, which requires the re-design of relay optics, and needs to consider the N.A. and SBP matching of different components due to the diffraction. We claim that our multiple cameras design can provide higher data transmission bandwidth, more flexible optical configurations and independent camera settings controlling. Such flexibilities cannot be achieved using a single lenslet array. Under current implementations, we have successfully demonstrated the acquisition of color light field videos for various fast-moving microscopic

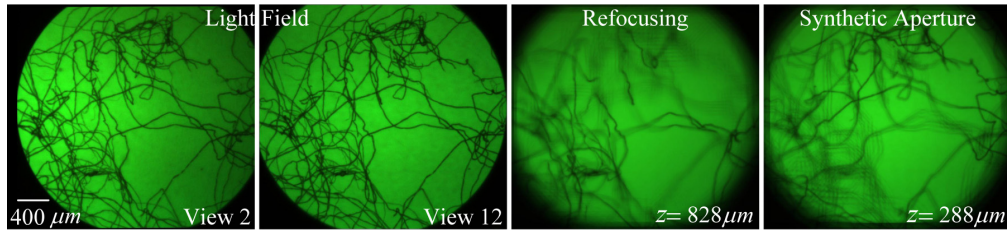


Fig. 7. Synthetic aperture and refocusing from the captured light field of cotton ([Visualization 7](#)). The aliasing is occurred in the refocusing and synthetic aperture results in this example due to the large-depth-range and thin-structure of the sample. We used all perspective images of the capture light field (first and second columns) for refocusing (third column) and adopted center 3×3 views for synthetic aperture (forth column).

specimens with a spatial resolution of 0.79 megapixels, angular views of 25, and a temporal resolution of 33 ms (30 fps). The data throughput of the our platform is 562.5 MB/s, 5 times higher than that of the latest commercial light field camera – Lytro Illum and the frame rate is 10 times faster. Lytro Illum has the 40 megapixels raw sensor resolution with only 3 fps temporal resolution (around 114.4 MB/s data transmission,), which limits its applications in imaging dynamic biological specimens, such as neural activities. We have demonstrated different applications of the reported platform, including higher resolution post-capture refocusing, phase reconstruction and 3D imaging of fast-moving microscopic samples. With our design, we hope to bridge the gap between computer vision and optics community so that various computer vision algorithms that based on multi-view or camera array can be applied to microscopy and facilitate various biological and metrological applications that require high-resolution, high-speed monitoring.

Yet, our current prototype has several limitations. First, the SBP of the Olympus objective imposes the limit angular resolution. Although the 5×5 angular resolution is good enough for most of the applications as presented, aliasing will occur when dealing with large-depth-range and thin-structures samples as an example shown in Fig. 7 ([Visualization 7](#)). In this example, the estimated depth range of the sample is 1.21 mm and the number of pixel shifting during the refocusing is $1.21 \text{ mm}/18.8 \mu\text{m} = 64$ for marginal views. Here, we used all perspective images for refocusing (third column) while adopting center 3×3 views for synthetic aperture (forth column). Such aliasing can be reduced by using angular interpolation or light field super-resolution method [13] under current implementation. We can also simply increase cameras by using a high SBP objective lens. Second, the field number of the Olympus IX73 camera port is smaller than the objective lens, which produces the edge resolution loss in this implementation and causes the image cropping of some marginal views. Using the microscope with larger field number could eliminate this problem. Third, the sensors are synchronized in software in our prototype, which can be implemented with external hardware trigger to achieve higher accuracy synchronization. Finally, the proposed prototype system is more expensive and bulkier compared with the single lenslet array based approach. However, the camera array is becoming widely used in macro-scenarios, such as the commercial product – Point Grey ProFUSION 25 (5×5 digital camera array), and we believe that our approach could be practical for microscopic imaging in the future.

5. Conclusion and future work

In summary, the proposed camera array based light field microscopy (CALM) can achieve high-resolution and high frame rate light field videos acquisition with high accuracy. We validated

the proposed approach with a standard commercial light microscope and demonstrated various applications by using the designed prototype system.

In the future, we would like to extend our approach to high-performance microscopy by combining views with different camera settings as a single view, such as high dynamic range imaging by setting different camera exposure times, and high speed imaging by staggering the camera trigger times. Furthermore, our method can be applied to fluorescence microscopy, and the axial and lateral resolution of light field can be further improved with 3D deconvolution algorithm for imaging the large-scale and high-speed neuronal activities in 3D [2, 5]. Combining Fourier ptychographic approach [9] for dynamic wide-field and high-resolution imaging is the other interesting avenue of future work.

Acknowledgments

This work was supported by the Project of NSFC (No. 61327902, No. 61120106003 and No. 61035002). The authors thank Yebin Liu and Gordon Wetzstein for insightful discussions, and Xiao Liu for the *C. elegans* used in this paper.